Med Biol Eng Comput (2018) 56:273–287
https://doi.org/10.1007/s11517-017-1686-y

ORIGINAL ARTICLE

A novel approach to an automated needle insertion in brachytherapy procedures

Ivan M. Buzurovic[1] · Slavisa Salinic[2] · Peter F. Orio[1] · Paul L. Nguyen[1] · Robert A. Cormack[1]

Received: 7 February 2017 / Accepted: 8 July 2017 / Published online: 15 July 2017

Abstract One of the most challenging phases in interstitial brachytherapy is the placement of the needles. In these medical procedures, the needles are inserted inside the tissue to guide the positioning of the radioactive sources. The low-dose-rate radioactive sources are placed inside the tissue permanently, whereas a radioactive source in the high-dose-rate brachytherapy is temporarily placed in the desired positions so that the delivery of the prescription dose to the clinical targets can be achieved. Consequently, the precise needle placement directly influences the radiation dose delivery and the treatment outcomes of patients. Any deviation from the desired position of the radioactive sources can cause a suboptimal dose distribution and inadequate tumor coverage. Therefore, it is of significant importance to develop a robust and sophisticated tool that can perform the automatic needle placement with a high level of accuracy for different medical procedures and conditions. In this study, we propose a novel concept for the automatic needle insertion using a new miniature automated robotic system. The mathematical model of this system was presented in detail, allowing the implementation of the model predictive control that can be used to govern the mechanism. The purpose of this approach was to minimize the lateral components of the generalized reactive force which is responsible for the tissue displacement and, consequently, for the needle deflection. The proposed approach was designed to predict and to compensate for the unmeasured disturbances, such as needle deflection or tissue resistance and reactive force, and it was capable of correcting them without waiting until the effect appears at the output of the system causing the needle deviation from the desired positions. The extensive simulation of the system was presented to evaluate the feasibility of the method and the parameters of interest including displacements, system errors and system responses to the change in the environmental conditions.

Keywords Mathematical modeling · Needle insertion · Robotic system · System simulation

1 Introduction

In contemporary brachytherapy, the accurate positioning of the needles into the predefined locations is a challenging and complex task due to a variety of reasons [9]. The precision and reproducibility of the needle placement in manual brachytherapy procedures are highly dependent on the experience and dexterity of the physicians [6]. Some of the major problems that appear during the needle insertion in brachytherapy are caused by the displacement and deformation of the soft tissue. Prostate deformation as well as possible calcifications within the gland or denser tumor tissue can cause needle deflection and needle clustering, which is hard to track and estimate. The lack of spatial resolution in ultrasound imaging or lack of the real-time needle position estimation in interstitial brachytherapy makes the implementation of the automatic corrections especially difficult. Needle deflection and displacement can result in significant dosimetric discrepancies in the clinical practice if the position error was not assessed and encountered. For instance, if the needle placement accuracy was ±1 mm,

✉ Ivan M. Buzurovic
ibuzurovic@lroc.harvard.edu

[1] Department of Radiation Oncology, Harvard Medical School, Boston, MA 02115, USA

[2] Department of Mechanics, Faculty of Mechanical and Civil Engineering, University of Kragujevac, Kraljevo 36000, Serbia

there exists a dose variation between 58 and 274% for a 40.7 cGy cm^2/h source of an HDR afterloader at the point located 2 mm distal to the tip of the needle, as previously reported in [36].

Several researchers have analyzed these problems. As a result, a variety of approaches were proposed to improve the insertion strategies [1, 3, 6, 15, 16, 18, 19, 32, 44]. Some of the suggested methodologies included the evaluation of different trajectories (such as curvilinear or flexible insertions), correlation of the tissue deformation and the infinitesimal force per tissue displacement for the real-time updates of the needle trajectories, or different models capable of predicting the deformation of the tissue caused by needle insertions, etc. However, the majority of these strategies have remained academic. Recently, several authors have reported the design, investigation and development of the image-guided robotic-based systems for the brachytherapy and biopsy procedures that included automatic needle insertions [11, 20, 24, 27, 29, 35, 38, 45]. The purpose of the listed systems was to accurately place the needles into the desired locations using robot-assisted automatic or semiautomatic insertions. To the best of our knowledge, none of these robotic systems is in clinical use.

The latest studies in this field reported some novel approaches to the accurate needle placement. They are briefly described to evaluate similarities and differences with our method. A comprehensive survey of the implemented needle insertion strategy was reported by Abolhassani [2]. In [25], the mutual effect of the stiff tungsten carbide trocar (a solid rod inside a cannula) combined with fast needle insertion was analyzed to decrease the needle deflection. In this article, it was found that the proper choice of the needle mechanism stiffness and needle insertion could decrease the deflection during the insertion procedures. This approach is similar to the one described in this article, but one more parameter was added to additionally increase the accuracy, i.e., the proper rotational velocity and acceleration of the needle. To achieve the accurate needle placement, some researchers included steering or the so-called curvilinear needle insertions. In [14], the authors presented the simulation of the needle insertion and steering methodology. A novel algorithm was capable of computing the contact force in real time. As described later, in our approach, we measure and predict the contact force to be able to decrease its lateral component and, consequently, the needle deflection. The modeling and simulation of the needle insertion play an important role in further investigation of the needle insertion effect on the soft tissue. A method that could estimate the force distribution was presented in [19]. In this approach to the needle position planning, no sensors were used, and the dynamic finite element method was used instead. The effects on friction between the needle and the tissue together with the needle tip characteristics such as the bevel angle, cone and triangle shapes were characterized in [31]. It was observed that the forces for needles with larger diameters were higher. In [23], the authors analyzed the tissue deformation and tissue displacement during breast biopsy to correlate the insertion accuracy and force. Many researchers found modeling of the insertion forces important since it is one of the main factors in the displacement of the needle. In [37], the force model for the robotic-assisted needle insertion was investigated. In an analysis of the robotic needle insertion, it was concluded that a higher level of accuracy could be achieved when different techniques for tissue fixation were used [43]. One of the advantages of the robotic needle insertions is the possibility to perform a variety of insertion strategies. Consequently, the parameters such as speed and/or acceleration during the procedure are changed during the procedure. The model in which the needle rotation was analyzed was developed and reported in [42]. The needle insertion procedure was characterized in a simulated environment using learning algorithms [21]. This study as well as the previously mentioned simulation studies proved the importance of the proper modeling and simulation for further development of the insertion strategies. On the basis of this concept and the related results [17], the researchers developed an interactive virtual needle insertion simulation using a robotic manipulator. The planning algorithm for the insertion of bevel-tip flexible needles was reported in [4]. The insertion plan for this purpose contained the desired needle location, needle orientation, bevel rotation and the distance from the targeted point inside the tissue. A comprehensive study of the robotic needle steering and its mechanical characteristics were presented in [28]. The modeling was performed using an energy-based method, followed by both the simulation and experimental results. The latest research results on this topic are reported in [5, 22, 34, 39, 41].

Considering the significance of the topic, we propose a novel approach to the automated needle insertion. Furthermore, we outlined the requirements for the development of a portable handheld $(n + 2)$ degree-of-freedom (DOF) automatic device for needle insertion. This device can incorporate the proposed insertion strategies with the goal to insert the needle with a high level of accuracy. To achieve this goal, we report the detailed mathematical model for the proposed system. The main purpose of the mathematical model approach was twofold: (a) the mathematical model should accurately represent the relevant physical phenomena that significantly influence the system dynamics of such device and (b) the mathematical model should be suitable for implementation in the real-time computations. Therefore, the presented mathematical model has a practical component rather than an academic value solely. In addition, the results were supported with extensive computer simulations. The proper choice of the

control methodology is crucial to achieve the accurate needle placement under different scenarios such as the variety of tissue responses to the insertion force, different lateral components of the forces to the needle and, consequently, the needle deflection. Ideally, the control method should be able to correct the needle deflection during the insertion, or to prevent the deflection by minimizing the lateral insertion forces. In the proposed method, we apply the model predictive control (MPC) as a possible control method capable of achieving the desired dynamical behavior of the system. The detailed implementation of the MPC prior to the simulation of the system was also presented in this article.

2 Methods and material

2.1 Concept description

Many medical procedures, such as LDR and HDR brachytherapy, required the accurate and timely delivery of needles inside the tissue for treatment of patients. As explained, the manual insertion is related to multiple challenges; however, the automated needle insertion research efforts [11, 20, 24, 27, 29, 35, 38, 45] are not clinically implemented—the developed platforms have remained research and academic efforts. One of the reasons for that was the complexity of such devices, complicated maintenance and implementation in only one type of insertion procedure. Having that in mind, we proposed a concept of the portable multipurpose device with a goal to achieve a high level of accuracy in various working regiments.

The purpose of this study is to investigate whether the automatic needle insertion using a proposed method implemented to the novel portable inserter of needles (PIN) is feasible and efficacious. The usage of the PIN should not be restricted to only one type of brachytherapy or biopsy procedures. The device should be able to operate with different types of needles in various procedures in which a needle insertion is required. In comparison with the manual insertion, the automatic needle insertion device should deliver the needles into the desired location more precisely within a shorter period of time. If the previous hypothesis can be proven, several direct benefits can be achieved. First, with the use of an automatic device for needle insertion, the number of CT/MRI scans during HDR interstitial brachytherapy can be decreased. The possible reduction in the number of scans is related to the increased accuracy of the needle placements; thus, the necessity for an iterative needle adjustment under CT guidance is eliminated. Consequently, the duration of time in which the patient is exposed to radiation during diagnostic exams (CT) can be decreased, and the patient may spend less time under anesthesia. Second, using an automatic device for needle insertion during LDR prostate seed implants can result in more favorable dosimetry.

Taking into account the reported findings related to the needle insertion, the brief description of the control methodologies capable of performing the desired tasks and the reasons for choosing the MPC were presented here. In our preliminary investigations, it was found that the adequate choice of the translational and rotational parameters (including speed and acceleration) could potentially decrease the deformation of the tissue and the target displacement by reducing the penetrating or insertion forces [7]. Therefore, it was observed that the penetrating force had a major influence on the needle insertion quality in the brachytherapy procedures. In [8], needle tracking was investigated during the automatic needle insertion, using the neural networks and their adaptive characteristics. A model capable of force prediction was developed to minimize the insertion force and, consequently, the needle displacement. Several advanced control strategies for needle insertion, such as force prediction, neural network predictive control (NNPC), proportional-integral-derivative controller (PID), and MPC, were analyzed in [6, 9, 11]. The MPC was shown to be most successful in minimizing the insertion force and needle deflection. The purpose of the previous method was to regulate the reactive force which was directly responsible for and proportional to the tissue displacement. The second control goal was to predict and compensate for the influence of the measured and unmeasured disturbances rather than to wait until the effect influences the output of the system by decreasing the accuracy. The unmeasured disturbances to the system can be complex reactive forces that appear during the needle–tissue interactions. If the reactive forces are minimized, the tissue displacement decreases. The prediction and control of the force were additionally used to minimize the effect of system latency. Due to the fact that this approach required an accurate mathematical model of the system, it was necessary to obtain a precise model of the needle mechanism during the insertion tasks.

2.2 Mathematical framework

To be able to perform the simulation of the system and to analyze the needle insertion parameters, the following steps were performed: (a) analysis of kinematics of the PIN, (b) development of the dynamic equations of motion for the PIN and (c) development and simulation of a kinematic and dynamic control algorithm using the MPC.

Figure 1a represents the model of the proposed mechanism with a needle named PIN. It consists of the needle holder 1 having mass m_1. The needle holder moves in the translational direction along the straight guidance rail. The model of the mechanism included a rotational part of the

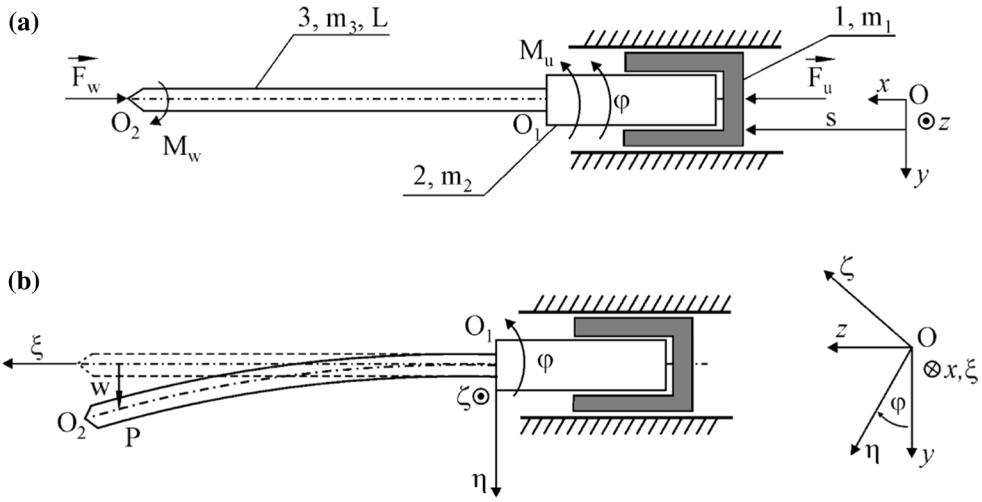

Fig. 1 **a** External schematic view of the mechanism with a needle (PIN), **b** the mechanism in the arbitrary moment during the needle insertion. The fixed and movable coordinate systems were presented

needle holder, marked as 2, having mass m_2 and axial inertia moment I_2 with respect to the rotational axes. The elastic needle 3 is the third part of the mechanism connected to the end O_1, and it is represented as a cantilever beam. In Fig. 1a, s denotes the motion of the needle holder 1 along the guiding rail, and φ is the rotational angle of needle holder 2. The control force F_u acts upon the holder and control torque M_u acts upon the rotational joint 2. During the needle insertion procedures, the resistant torque M_w acts against the needle rotation as well as resistant force F_w that acts upon the needle tip O_2, as shown in Fig. 1a. It is assumed that the force F_w is parallel to the axis x during the motion of the needle.

The needle itself is represented as an elastic beam with n DOF. With this purpose in mind, the analyzed mechanical system has indefinite degrees of freedom. Since the mechanism consists of rigid and elastic bodies, the system belongs to the group of hybrid systems. The dynamical behavior of such systems is represented with both differential equations and partial differential equations. To increase the real-time calculations without losing precision, the methodology called the assumed-modes method was used for the mathematical modeling [26]. In this approach, the dynamics of the elastic needle was analyzed using a finite number of degrees of freedom. The configuration of the mechanism at the arbitrary moment during the needle insertion is presented in Fig. 1b. The frame O_{xyz} is the inertial frame of reference with O_{xy} representing a vertical plane. The moving coordinate frame $O_1\xi\eta\zeta$ is fixed to body 2 in such manner that the axis ξ coincides with the needle axis in its non-deformed configuration.

To develop a mathematical model of the proposed system (PIN), the following assumptions are adopted: (a) the axial and torsion deformations of the individual segments of the needle are neglected; (b) the central line of the deformed needle is the plane curve lying in the plane $O_1\xi\eta$ (bending deformation of the needle around only one principal axis of the cross section); (c) the small deformations of the needle are analyzed; (d) the dynamics of the needle is considered in the frame of the Euler–Bernoulli beam theory.

When the insertion procedure is analyzed, it can be concluded that all adopted assumptions describe the realistic situations during needle insertions [6–9]. For instance, the needle does not elongate or twist during the insertion (assumption (a)), or the needle never deforms in three planes, as assumed in (b). Assumptions (c) and (d) represent the methodology undertaken for the mathematical modeling.

The position vector $\mathbf{r}$ with respect to frame O_{xyz} of the arbitrary point P on the central line of the deformed needle can be written as:

$$\mathbf{r} = \mathbf{p} + \mathbf{R}\mathbf{w} \tag{1}$$

where $\mathbf{p} = [s(t) + \xi, 0\ 0]^T$ is the position vector of the point P with respect to the frame O_{xyz} in the non-deformed state of the needle; $\mathbf{w} = [0, w(\xi, t), 0]^T$ is the deformation vector defined in the local frame $O_1\xi\eta\zeta$ (the central line of the deformed needle is in plane $O_1\xi\eta$), and $\mathbf{R}$ is the transformation matrix from the local frame $O_1\xi\eta\zeta$ to the inertial frame O_{xyz}, which can be written as:

$$\mathbf{R} = \begin{bmatrix} 1 & 0 & 0 \\ 0 & \cos\varphi & -\sin\varphi \\ 0 & \sin\varphi & \cos\varphi \end{bmatrix}. \tag{2}$$

Based on the assumed-modes method, the lateral displacement $w(\xi; t)$ of the central line of the needle can be represented by the finite series

$$w(\xi, t) = \sum_{i=1}^{n} \left(\boldsymbol{\Phi}_i\right) q_{if}(t) \tag{3}$$

where $\boldsymbol{\Phi}_i(\xi)(i = 1, \ldots, n)$ are the modal functions, $q_{if}(t)(i = 1, \ldots, n)$ are the modal generalized coordinates, and n is the number of modes used in the computation. In this regard, the motion of the mechanism shown in Fig. 1b can be approximately described by $n + 2$ generalized coordinates $\mathbf{q} = \left[\mathbf{q}_r^T, \mathbf{q}_f^T\right]^T$, where $\mathbf{q}_r = [s, \varphi]^T$ and $\mathbf{q}_f = \left[q_{1f}, q_{2f}, \ldots, q_{nf}\right]^T$.

The first derivative of the vector $\mathbf{r}$ with respect to the time t is

$$\dot{\mathbf{r}} = \dot{\mathbf{p}} + \frac{\partial \mathbf{R}}{\partial \varphi}\mathbf{w}\dot{\varphi} + \mathbf{R}\dot{\mathbf{w}} \tag{4}$$

or, taking into account (3), in a developed form

$$\dot{\mathbf{r}} = \begin{bmatrix} \dot{s} \\ \sum_{i=1}^{n} \boldsymbol{\Phi}_i(\xi)\left(-\dot{\varphi} q_{if}(t) \sin\varphi + \dot{q}_{if}(t)\cos\varphi\right) \\ \sum_{i=1}^{n} \boldsymbol{\Phi}_i(\xi)\left(\dot{\varphi} q_{if}(t) \cos\varphi + \dot{q}_{if}(t)\sin\varphi\right) \end{bmatrix}. \tag{5}$$

The kinetic energies (T) of bodies 1 and 2 are, respectively,

$$T_1 = \frac{1}{2} m_1 \dot{s}^2 \tag{6}$$

and

$$T_2 = \frac{1}{2} m_2 \dot{s}^2 + \frac{1}{2} I_2 \dot{\varphi}^2 \tag{7}$$

The kinetic energy of the needle may be computed as

$$T_3 = \frac{1}{2}\int_0^L \rho A \dot{\mathbf{r}}^T \dot{\mathbf{r}} \mathrm{d}\xi \tag{8}$$

where ρ, A and L are mass density, cross-sectional area of the needle and length of the needle, respectively. When relation (5) is inserted into Eq. (8), and Eqs. (6) and (7) are taken into account, the following expression for the total kinetic energy is obtained:

$$\begin{aligned} T = T_1 + T_2 + T_3 = {} & \frac{1}{2}(m_1 + m_2)\dot{s}^2 + \frac{1}{2} I_2 \dot{\varphi}^2 \\ & + \frac{1}{2}\int_0^L \rho A \left[\dot{s}^2 + \sum_{i=1}^{n}\sum_{j=1}^{n} \boldsymbol{\Phi}_i(\xi)\boldsymbol{\Phi}_j(\xi)\left(-\dot{\varphi} q_{if}(t)\sin\varphi + \dot{q}_{if}(t)\cos\varphi\right)\left(-\dot{\varphi} q_{jf}(t)\sin\varphi + \dot{q}_{jf}(t)\cos\varphi\right)\right]\mathrm{d}\xi \\ & + \frac{1}{2}\int_0^L \rho A \left[\sum_{i=1}^{n}\sum_{j=1}^{n} \boldsymbol{\Phi}_i(\xi)\boldsymbol{\Phi}_j(\xi)\left(\dot{\varphi} q_{if}(t)\cos\varphi + \dot{q}_{if}(t)\sin\varphi\right)\left(\dot{\varphi} q_{jf}(t)\cos\varphi + \dot{q}_{jf}(t)\sin\varphi\right)\right]\mathrm{d}\xi. \end{aligned} \tag{9}$$

The potential energy (V) of the needle caused by bending deformation is:

$$V = \frac{1}{2}\int_0^L EI_\zeta \left(\frac{\partial^2 w}{\partial \xi^2}\right)^2 \mathrm{d}\xi \tag{10}$$

or, taking into account Eq. (3),

$$V = \frac{1}{2}\sum_{i=1}^{n}\sum_{j=1}^{n}\left(\int_0^L EI_\zeta \boldsymbol{\Phi}_i''(\xi)\boldsymbol{\Phi}_j''(\xi)\mathrm{d}\xi\right) q_{if}(t) q_{jf}(t) \tag{11}$$

where E is the Young's modulus, I_ζ is the area moment of inertia of the cross section around the axis ζ, and the double prime denotes the second derivation with respect to coordinate ξ.

The virtual work of the non-conservative forces is:

$$\delta A = -F_w \delta s - M_w \delta\varphi. \tag{12}$$

The corresponding non-conservative parts of generalized forces are:

$$\begin{aligned} \boldsymbol{Q}_r &= \left[Q_s,\ Q_\varphi\right]^T = \left[-F_w,\ -M_w\right]^T, \\ \boldsymbol{Q}_f &= \left[Q_{q_{1f}},\ Q_{q_{2f}}, \ldots,\ Q_{q_{nf}}\right]^T = \mathbf{0}_{n\times 1} \end{aligned} \tag{13}$$

where $\mathbf{0}_{n\times 1} \in R^{\times 1}$ is a zero matrix.

According to [40], the eigenfunctions can be chosen for a cantilever beam for mode functions. These functions have the following form as described in [24]:

$$\boldsymbol{\Phi}_i(\xi) = u_i\left[\sin\beta_i\xi - \sinh\beta_i\xi - \frac{\sin\beta_i L + \sinh\beta_i L}{\cos\beta_i L + \cosh\beta_i L}\left(\cos\beta_i\xi - \cosh\beta_i\xi\right)\right] \tag{14}$$

where $u_i(i = 1, \ldots, n)$ are constant and β_i are the roots of the following frequency Eq. [24]:

$$\cos\beta_i L \cosh\beta_i L = -1. \tag{15}$$

For example, the first three eigenvalues are: $\beta_1 L = 1.8751$, $\beta_2 L = 4.6941$ and $\beta_3 L = 7.8548$. The constants u_i are chosen so that the following condition is satisfied

$$\int_0^L \boldsymbol{\Phi}_i^2(\xi)\mathrm{d}\xi = L. \tag{16}$$

The eigenfunctions (14) possess the orthogonality property [24], that is:

$$\int_0^L \rho A \boldsymbol{\Phi}_i(\xi)\boldsymbol{\Phi}_j(\xi) = 0, \quad i,j = 1,2,\ \ldots, n; \quad i \neq j \tag{17}$$

Based on Eqs. (16) and (17), the expression for the total energy (9) takes the following form:

$$T = \frac{1}{2}(m_1 + m_2 + m_3)\dot{s}^2 + \frac{1}{2}\left[I_2 + \sum_{i=1}^{n} m_3 q_{if}^2(t)\right]\dot{\varphi}^2 + \frac{1}{2}\sum_{i=1}^{n} m_3 \dot{q}_{if}^2(t) \tag{18}$$

or in the matrix form

$$T = \frac{1}{2}\begin{bmatrix}\dot{\mathbf{q}}_r^T & \dot{\mathbf{q}}_f^T\end{bmatrix}\begin{bmatrix}\mathbf{M}_{rr} & 0_{2\times n}\\ 0_{n\times 2} & \mathbf{M}_{ff}\end{bmatrix}\begin{bmatrix}\dot{\mathbf{q}}_r\\ \dot{\mathbf{q}}_f\end{bmatrix} \tag{19}$$

where $\boldsymbol{M}_{rr} = \mathrm{diag}\left(m_1 + m_2 + m_3, I_2 + \sum_{i=1}^{n} m_3 q_{if}^2(t)\right)$, $\boldsymbol{M}_{ff} = m_3 \boldsymbol{I}_{n\times n}$, $\boldsymbol{I}_{n\times n} \in R^{n\times n}$ is an identity matrix, and $\mathbf{0}_{2\times n} \in R^{2\times n}$ and $\mathbf{0}_{n\times 2} \in R^{n\times 2}$ are zero matrices.

It can be shown that, for the cantilever beam, the orthogonality relations (17) can be represented in the following alternative form [26]:

$$\int_0^L EI_\zeta \boldsymbol{\Phi}_i''(\xi)\boldsymbol{\Phi}_j''(\xi)\mathrm{d}\xi = 0, \quad i,j = 1,2,\ \ldots, n; \quad i \neq j. \tag{20}$$

Based on this equation, the expression for the potential energy (11) is reduced to the following form:

$$V = \frac{1}{2}\sum_{i=1}^{n}\left(\int_0^L EI_\zeta(\boldsymbol{\Phi}_i''(\xi))^2\mathrm{d}\xi\right)q_{if}^2(t) \tag{21}$$

or equivalently, in the matrix form:r

$$V = \frac{1}{2}\begin{bmatrix}\mathbf{q}_r^T & \mathbf{q}_f^T\end{bmatrix}\begin{bmatrix}0_{2\times 2} & 0_{2\times n}\\ 0_{n\times 2} & \mathbf{K}\end{bmatrix}\begin{bmatrix}\mathbf{q}_r\\ \mathbf{q}_f\end{bmatrix} \tag{22}$$

where $\mathbf{0}_{2\times 2} \in R^{2\times 2}$ is a zero matrix and $K = \mathrm{diag}\left(\int_0^L EI_\zeta(\boldsymbol{\Phi}_1''(\xi))^2\mathrm{d}, \ldots, \int_0^L EI_\zeta(\boldsymbol{\Phi}_n''(\xi)\right)^2\mathrm{d}\xi\ )$.

Finally, the differential equations of the motion of the system considered can be obtained by means of the Lagrange equation [12],

$$\frac{\mathrm{d}}{\mathrm{d}t}\left(\frac{\partial L}{\partial \dot{\mathbf{q}}_r}\right) - \frac{\partial L}{\partial \mathbf{q}_r} = \mathbf{Q}_r \tag{23}$$

$$\frac{\mathrm{d}}{\mathrm{d}t}\left(\frac{\partial L}{\partial \dot{\mathbf{q}}_f}\right) - \frac{\partial L}{\partial \mathbf{q}_f} = \mathbf{Q}_f \tag{24}$$

where $L = T - V$ is the Lagrangian function. Equations (23) and (24) can be written in the following matrix form:

$$\begin{bmatrix}\mathbf{M}_{rr} & \mathbf{0}_{2\times n}\\ \mathbf{0}_{n\times 2} & \mathrm{M}_{ff}\end{bmatrix}\begin{bmatrix}\ddot{\mathbf{q}}_r\\ \ddot{\mathbf{q}}_f\end{bmatrix} + \mathbf{h}\left(\dot{\mathbf{q}}_r, \dot{\mathbf{q}}_f, \mathbf{q}_f\right) + \begin{bmatrix}\mathbf{0}_{2\times 2} & \mathbf{0}_{2\times n}\\ \mathbf{0}_{n\times 2} & \mathbf{K}\end{bmatrix}\begin{bmatrix}\mathbf{q}_r\\ \mathbf{q}_f\end{bmatrix} = \begin{bmatrix}\mathbf{Q}_r\\ \mathbf{Q}_f\end{bmatrix} \tag{25}$$

where

$$\mathbf{h}\left(\dot{\mathbf{q}}_r, \dot{\mathbf{q}}_f, \mathbf{q}_f\right) = [0, 2m_3\left(\sum_{i=1}^{n} q_{if}\dot{q}_{if}\right)\dot{\varphi}, - m_3 q_{1f}\dot{\varphi}^2, -m_3 q_{2f}\dot{\varphi}^2, \ldots, - m_3 q_{nf}\dot{\varphi}^2]^T R^{(2+n)\times 1}.$$

This model represents the basis for the development of the needle insertion control that has to minimize the lateral insertion force and needle deflection. The model does not incorporate the potential energy of the needle due to gravity force since it does not influence the overall system dynamics.

Finally, the system (25) can be transformed to a nonlinear state-space form [10] as follows:

$$\begin{aligned}\dot{\mathbf{x}}(t) &= A(t)\mathbf{x}(t) + B(t)\mathbf{u}(t) + \mathbf{v}(t)\\ \mathbf{y}(t) &= C(t)\mathbf{x}(t) + \mathbf{w}(t),\end{aligned} \tag{26}$$

where $\mathbf{x}(t)$, $\mathbf{u}(t)$ and $\mathbf{y}(t)$ are state vector, control vector and output vector, respectively; $\mathbf{v}(t)$ and $\mathbf{w}(t)$ are state disturbance and measured disturbance vectors; $A(t)$, $B(t)$ and $C(t)$ are corresponding time varying state matrix, input matrix and output matrix, respectively. Following the procedure reported in [10], the matrices $A(t)$, $B(t)$ and $C(t)$ are calculated as: $A(t) = [\mathbf{0\ 0}\ \boldsymbol{I}\ \mathbf{0;\ 0\ 0\ 0}\ \boldsymbol{I}\mathbf{;\ 0\ 0\ 0\ 0;\ 0\ K/M}_{\boldsymbol{ff}}\ \mathbf{0\ 0}]$, $B(t) = [\mathbf{0\ 0\ 1/M}_{\boldsymbol{rr}}\ \mathbf{1/M}_{\boldsymbol{ff}}]^T$, and $C(t)$ is equal to identity matrix since the generalized positions and velocities are chosen to be the system output. In addition, $\mathbf{x}(t) = [\mathbf{x_1\ x_2\ x_3\ x_4}]^T$, $\mathbf{x_1} = \mathbf{q}_r$, $\mathbf{x_2} = \mathbf{q}_f$, $\mathbf{x_3} = \dot{\mathbf{q}}_r$, and $\mathbf{x_4} = \dot{\mathbf{q}}_f$. Consequently, $\mathbf{v}(t) = [\mathbf{0\ 0\ 0\ -h_1(x_2, x_3, x_4)}]^T$, where $\mathbf{h_1(x_2, x_3, x_4)}$ is the second element of the $\mathbf{h}\left(\dot{\mathbf{q}}_r, \dot{\mathbf{q}}_f, \mathbf{q}_f\right) = [0, \mathbf{h}_1\left(\dot{\mathbf{q}}_r, \dot{\mathbf{q}}_f, \mathbf{q}_f\right)]$ transformed to its state-space form.

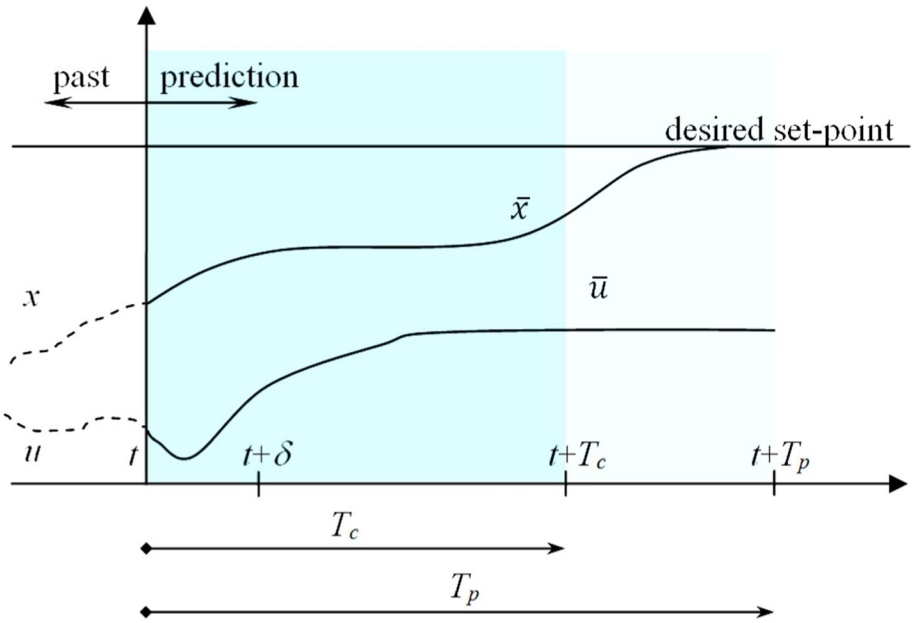

Fig. 2 General representation of the MPC functionality

2.3 Control scheme

The MPC operates by finding the adequate control solution in an iterative process, incorporating the system dynamics, measurements and disturbances into the calculations. The schematic representation of the process is presented in Fig. 2. In this specific case, the formulation of the control procedure is as follows: based on the measurements of the resistance force F_w that acts upon the needle tip, the controller predicts the system behavior over the prediction horizon T_p, and calculates the input (F_u and M_u) of the system over the control horizon T_c. This calculation is performed such that the performance objective is minimized. In this case, the lateral displacement of the needle **Rw**, as in Eq. (1), is minimized.

Consequently, the basic task of the MPC is to calculate the insertion speed represented by the motor driving force F_u, and the rotational speed of the needle represented by the motor driving torque M_u so that the lateral displacements of the needle tip and the lateral components of the insertion force over the sampling period can be minimized. This calculation is performed iteratively in real time to allow for the needle steering with variable translational and rotational speeds. In the case when the lateral force components and the lateral displacement are zero, the controller continues to operate, using the same parameters until the desired behavior is maintained. The sampling time δ can vary to save the calculation time, but it is usually set to be fixed. The calculated system states at the instant $t + \delta$ let both the control procedure and the prediction horizon move forward. For this case, the linear model of the system would be insufficient to describe the process adequately; therefore, a nonlinear model was used for a more accurate representation of the process.

The overall purpose of the control task is to change the control parameters, such as the rotational and translational speed, and to obtain the rectilinear insertion makes the reference constant. In this work, we analyze a more

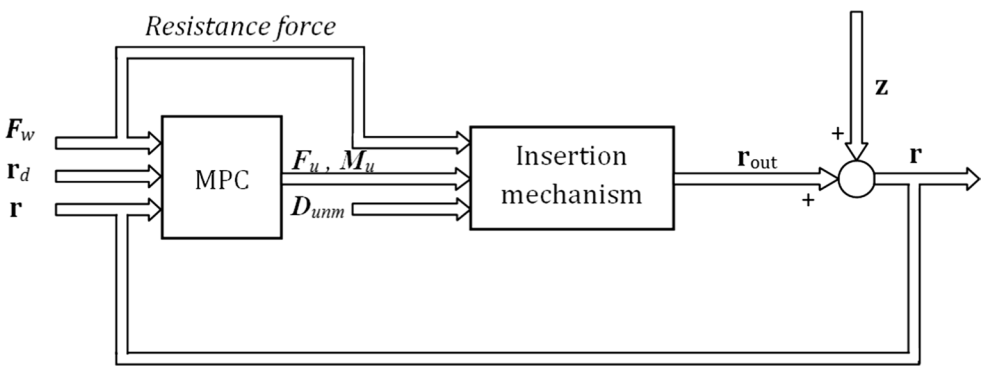

Fig. 3 Block diagram of the MPC for the needle insertion procedure using a proposed mechanism

conservative case—rectilinear needle insertion; however, this reference does not need to be constant and the system is potentially capable of needle steering in the 3D space. In general, to allow for the optimal needle placement inside the tissue for the brachytherapy procedures, we propose to minimize the lateral components of the insertion force (resistance force), and to predict and compensate for the influence of both the measured and unmeasured disturbances before their effect influences the system behavior, i.e., needle displacement from the desired position. With this control strategy, it is possible to minimize both forces during the insertion and lateral displacement and, consequently, the needle deflection. The system receives information about the measured reactive force and tunes the parameters such as the translational speed and needle rotation in real time during the insertion.

Referring to Fig. 3, the following parameters and variables are represented in the block diagram: D_{unm} represents the unmeasured disturbances to the system. These disturbances, such as the tissue resistance or lateral forces, increase the needle deflection during the procedure. The deflection depends on the insertion force, and based on that value, it can be estimated with a satisfactory level of accuracy, as in [7]. $\mathbf{r}_d$ is the vector that represents all reference position values, i.e., the desired needle tip position, during the insertion. This value is the targeting value of the output. The task of the system is to decrease the lateral components of the actual insertion force in order to minimize the deflection and, consequently, to meet the criteria for this set point. The resistance force F_w is a measured disturbance of the system for which the MPC provides a feedforward compensation in order to decrease its influence on the needle position. F_u and M_u are the generalized torques of the motors, as previously described. These control signals are adjusted in real time to achieve the objectives of the system. The output of the systems is denoted as $\mathbf{r}_{\text{out}}$, and it is a real needle tip position during the insertion. This value is a controlled variable of the system. $\mathbf{r}$ is the output of the system, i.e., the calculated tip position that was used for the estimation of $\mathbf{r}_{\text{out}}$. The signal $\mathbf{z}$ represents the disturbance vector that contains the unpredicted influences on the system. The disturbance vector includes the electrical and actuator noises, calibration uncertainties and inaccuracies due to the modeling of the physical system as well as other unpredicted effects on the system.

The described approach is challenging and highly dependent on the accuracy of the mathematical model of the process. That is the basic reason why the equation of the motion (25) is crucial for further development. The second challenge in this approach is the proper individual tuning of the parameters, such as the adjustments of the actuators and the selection of the proper weights to allow for a minimal deviation of the desired deflection over its set points within the prediction horizon.

2.4 Model predictive controller

In the situation when complicated physical processes related to needle tissue interaction are analyzed, two opposite requirements arouse: the possibility of the development of an accurate mathematical model and, on the other hand, the possibility to implement the proposed method to the real-time procedure with highly demanded data processing and computation. The insertion procedure should be performed only in few seconds. The most suitable controller for such tasks should be capable of minimizing the influence of the unknown system disturbances and deviations in mathematical modeling, while obtaining the measurements from the environment for the corrected control output. Therefore, it was decided to use a model predictive controller (MPCN). The MPCN is the key component of the proposed system. The proposed controller was capable of predicting and compensating for the unmeasured disturbances, such as the needle deflection or tissue reactive force, and it was capable of correcting them without waiting until the effect appears at the output of the system. On the other hand, the controller was capable of maintaining the desired needle tip position within the predefined limits, allowing for a high level of accuracy. Since the system model (25) is the system of a differential nonlinear equation, the MPCN is also nonlinear. It means that this approach required the iterative solution of an optimal control problem.

In this part, the basic functionality of the MPC is described. Initially, the MPC controller solves the linear-quadratic-Gaussian optimization problem for our multi-input multi-output system. For the system (25), the following cost function has been minimized

$$J = E\left(\mathbf{x}^T(T)F\mathbf{x}(T) + \int_0^T \left(\mathbf{x}^T(t)Q(t)\mathbf{x}(T) + \mathbf{u}^T(t)R(t)\mathbf{u}(T)\right)\mathrm{d}t\right) \tag{27}$$

where E denotes the vector of the reference values or set points; T is the time horizon that can be finite or equal to $+\infty$, depending on the time during which it is necessary to perform the insertion of the individual needle. When $T\rightarrow+\infty$, $\mathbf{x}^T(T)F\mathbf{x}(T)0$. The goal of the optimization process is to find the feedback gain matrix $L(t)$, i.e., the proper torques for the motors that will guarantee the desired dynamic behavior of the system. Consequently,

$$L(t) = R^{-1}(t)B^T(t)S(t) \tag{28}$$

where $S(t)$ is the solution of the following Riccati differential equation:

$$\dot{S}(t) = -A^T(t)S(t) - S(t)A(t) + S(t)B(t)R^{-1}(t)B^T(t)S(t) - Q(t) \quad (29)$$

The control algorithm with multiple variables uses the optimization function (30) together with the internal dynamics (25) of the system. For the control process, the information about the past controlled motions was used to calculate the optimal dynamical behavior during insertion.

$$J = \sum_{i=1}^{N} w_{x_i}(r_i - x_i)^2 + \sum_{i=1}^{N} w_{u_i} u_i^2 \quad (30)$$

where x_i is the needle tip position, r_i is the reference needle tip position, u_i is the control signal from the actuators, w_{x_i} is the weighting coefficient responsible for the relative importance of the x_i, whereas w_{u_i} is the weighting coefficient that penalizes the large change in gradient of u_i.

Thus, the optimization cost function with the proper choice of the coefficients (30) ensures the decay of the transient errors as well as the reduction in the steady-state errors.

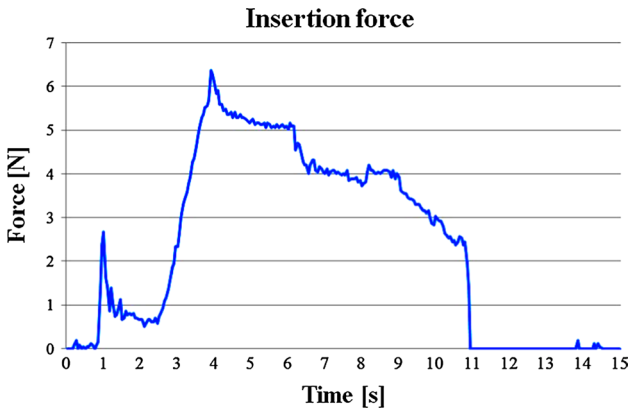

Fig. 4 Measured axial insertion force at the proximal end of the needle used in the simulation (a representative case)

2.5 Measured output

The rigorous simulation of the system (26) required the measuring force that was previously collected and implemented into the procedure.

The force was measured in vivo using single-axis force sensors (Model 13, Honeywell Sensotech, Columbus, OH) and a 6-axis force-torque sensor (Nano17, ATI Industrial Automation, Apex, NC). The first sensor was placed proximally, and it collected the axial insertion force at the needle tip. The second sensor was placed at the distal end of the mechanism, and it collected both the force and the components at each segment n of the needle during the insertion, as in [7]. The graphical representation of these signals is presented in Figs. 4 and 5. The force dataset was chosen to correspond to the realistic clinical scenario, so the proposed system was simulated using the force values obtained during the needle insertion in both the experimental and the clinical environments using phantom and animal/human studies [6–9].

The collected data served as a measured output, i.e., the resistance force during the simulation, and the forces and torques were used to assess the needle deflection changes during the simulation procedures.

2.6 Case study

In this case, we use the mathematical model of the $(n + 2)$ DOF needle insertion mechanism (25) and a model predictive controller (MPCN) to simulate the insertion procedure. When the cost function (30) is minimized, the lateral force components are reduced. With the monitoring of the axial insertion force, the needle deflection is minimized, and the needle tip should be at the predefined desired position. This hypothesis was investigated in the rigorous computer simulation. The prediction of the insertion force was analyzed as well.

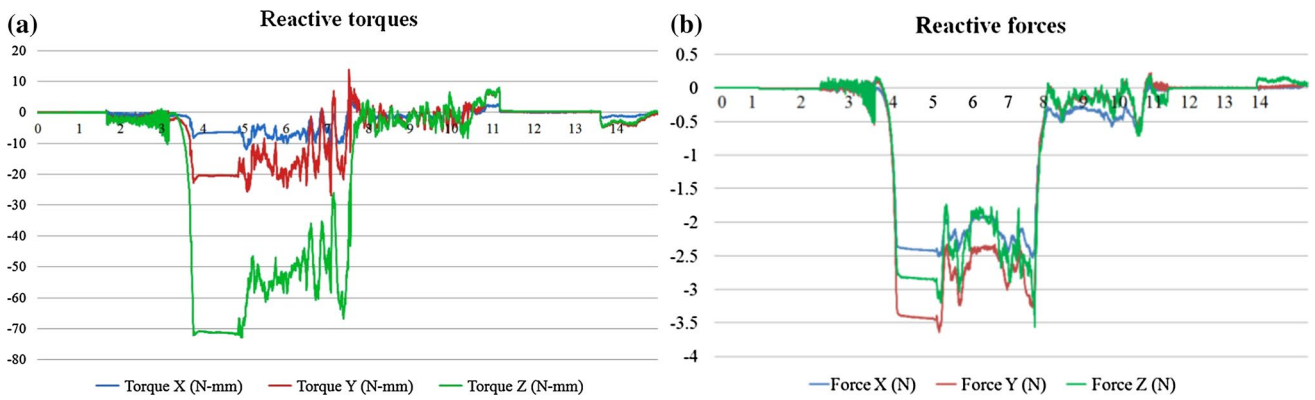

Fig. 5 Needle insertion parameters: **a** reactive forces in x, y and z directions, and **b** reactive torques on x, y and z axes (a representative case)

2.7 Simulation parameters

During the simulation phase, we investigated the needle deflection and deformation for variable velocities of the needle translation and rotation during the insertion, based on the readings from the force sensor and the tip position measurements related to the lateral needle deformation. The translational velocity range was 5–120 mm/s, and the needle rotation range was 0–30 rev/s. In this case, the arbitrary point P described in Eq. (1) was chosen to be a point at the needle tip. For the computer simulation, the initial control parameters or their ranges for the needle insertion were chosen as in [7]: the initial needle translational speed was 40 mm/s, and the initial rotational speed was 8 rev/s. The prediction horizon was $T_p = 200$ ms; the control horizon was $T_c = 150$ ms; and the sampling time was $\delta = 50$ ms. The needle holder mass was $m_1 = 0.10$ kg, while the rotational joint head mass was $m_2 = 0.05$ kg, and the needle mass was $m_1 = 0.02$ kg; the needle length was $L = 0.2$ m. The simulation was performed with the parameters of the cannula Rev. A4, 304 Stainless steel needle ($r = 2.98$ mm $\pm$ .01 mm with a bevel angle of 15°) and for the stylet Rev. A4, 304 Stainless steel needle (Vita Needle Company, Needham, MA USA). The number of nodes used in the computation was $n = 20$. The length of each node was $L_n = 0.01$ m. The system delay in the prediction algorithm is $t_d = 50$ ms. The tap number for the different x, y and z axes is $t_X = 1$, $t_Y = 1$ and $t_Z = 2$. The learning rate in the prediction algorithm for x, y and z axes is $\mu_{\cdot X} = 1.3$, $\mu_{\cdot Y} = 1.4$ and $\mu_{\cdot X} = 1.7$

The implementation of the MPC was performed using deliberately written C/C++ functions embedded into MATLAB (Natick, MA, USA) API libraries suitable for handling such multivariable systems. The optimization problem (29), (30) was solved within the chosen sampling period after the libraries were compiled and optimized. The first element of the control vector was calculated, and the further calculation was done in each sampling instant keeping the prediction horizon of the same length so that the optimal control vector should be obtained in real time. Since the state prediction (vector values $\mathbf{x}(t)$) depends on the measured values (Fig. 4), this process introduces the feedback into the MPCN, assuring the robustness to modeling errors and uncertainties. The simulation of the system was performed with several types of disturbances and their magnitudes (signal $\mathbf{z}$) including white nose with zero mean and unit variance, random step-like and ramp-like and disturbances. For the white noise disturbance, the static gain was used. For the step-like and ramp-like disturbances, one and two integrators with static gains were used, respectively.

3 Results

3.1 Insertion accuracy

The insertion accuracy was evaluated when the MPCN governed the needle insertion system represented by Eq. (25). A representative case of the needle tip trajectory

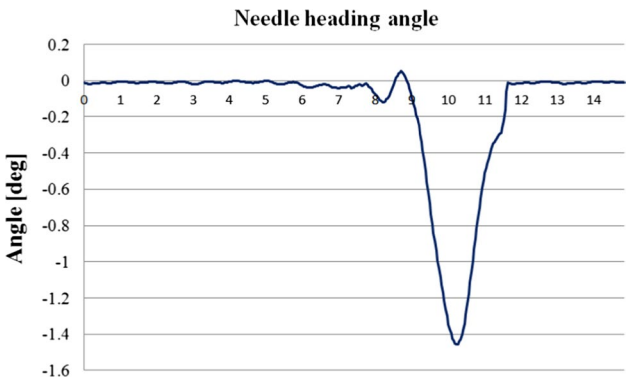

Fig. 7 Heading angle during insertion; MPCN corrects for the possible increase in the angle

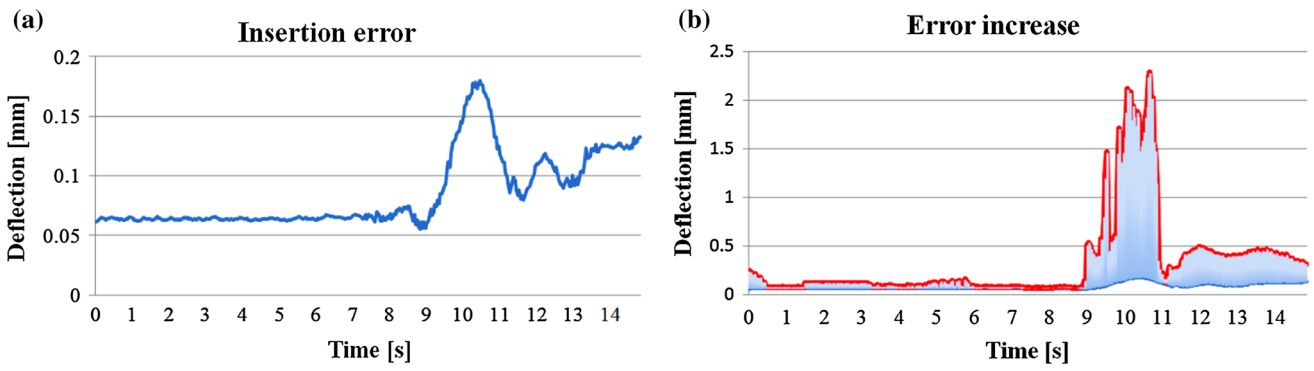

Fig. 6 Needle deflection **a** with and **b** without rotation control component (a representative case). An increase in the error was noticed when the needle rotation was not included into the process (*marked region*)

is presented in Fig. 6. Under the influence of the measured force, it was revealed that it was possible to minimize the needle deflection and to insert the needle into the desired position with the highest level of accuracy when the MPC approach was used. Additionally, Fig. 6 shows the simulation results when the $M_u = 0$, i.e., when the actuator dedicated to the needle rotation was turned off.

The simulation was performed under the influence of the recorded forces as in Fig. 5. This conclusion proved the concept that the control of the translational motion was not sufficient and could not minimize the deflection up to the level at which the needles would not deflect significantly. Consequently, in this simulation, we proved the importance of the needle rotation for the accurate needle placement. When the simulation was repeated for different insertion depths (from 4 to 10 cm), it was revealed that the average needle tip displacements in the x, y and z directions were, -0.09 , 0.19 and 0.12 mm with an average SD = 0.13 mm, respectively.

The auto-correction of the needle heading angle is presented in Fig. 7. It was observed that the angle increased initially before the MPCN started to correct the lateral displacement and, consequently, to minimize the angle.

3.2 Insertion force calculations

At this point, when the needle tip displacement is known, it is possible to use Eqs. (1) and (3) to recalculate the insertion forces. The values of the actuator parameters that lead to the insertions with minimal deflections are known as well. With the forward kinematics calculations of the system model, it is possible to calculate and re-evaluate the insertion forces achieved in the simulations. For this purpose, we recalculated the forces and the torques presented in Fig. 5 to evaluate whether this process would result in any change in the measured insertion parameters. The results are presented in Fig. 8.

It was noticed that the torque on the insertion axis (z) did not change significantly, whereas the x and y torques were minimized. This result was to be expected

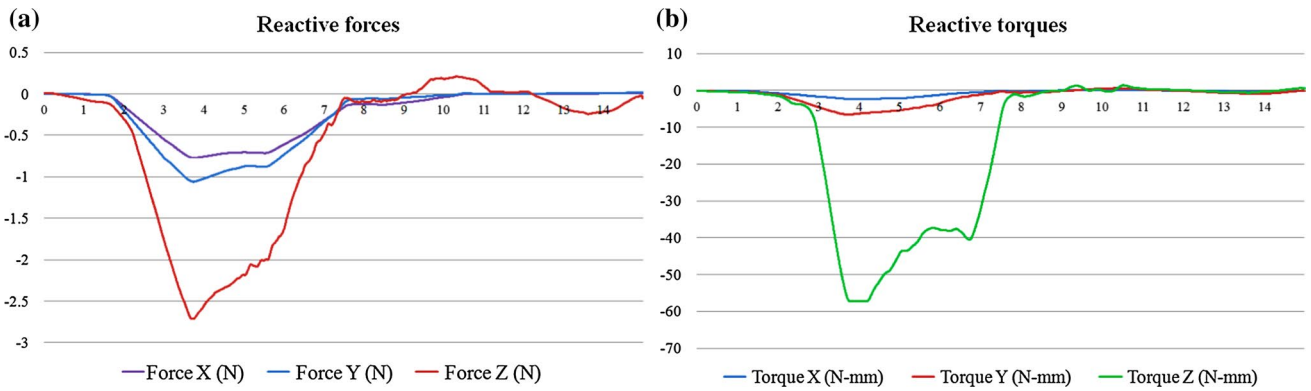

Fig. 8 Recalculated needle insertion parameters: **a** reactive forces in x, y and z directions, and **b** reactive torques on x, y and z axis (a representative case)

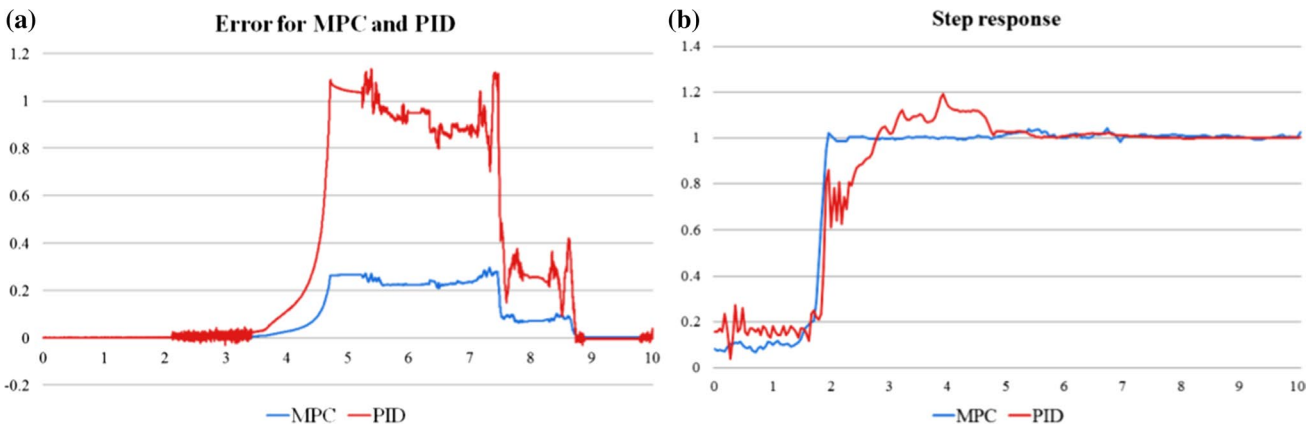

Fig. 9 **a** Position error and **b** step response for MPC and PID needle control (a representative case)

only if the lateral displacement of the needle was minimized. The torque on the insertion axis was not changed since it was necessary to apply the torque to allow for the needle insertion and steering. The similar observation was noticed in the case of the insertion force recorded at variable points of the needle during the procedures.

3.3 Comparison between MPC and PID control methodologies

We compared the needle tip position accuracy to the accuracy achieved by the commonly used control strategies to evaluate the insertion accuracy when the MPC control approach and MPCN were used. The insertion system (Fig. 1) described by a mathematical model (25) was simulated using both the MPCN and the PID to evaluate the increase in accuracy when the MPC was used. The results are presented in Fig. 9.

It was noticed that the needle positioning accuracy was higher with the MPC method due to the needle steering provision, i.e., the adaptive change in the control parameters such as the velocity and rotational speed of the needle. When the response of both systems to the step function was evaluated, it was noticed that the transient parameters such as overshoot and settling time were more favorable in the MPC case. Whereas it is know that the PID ensures the asymptotic decay of the transient errors as well as reduction in the steady-state errors, the MPCN is capable of dealing with the overall system error without waiting until the effect appears at the output of the system regardless of whether the error is caused by the different modeling approaches or other unknown influences on the analyzed system.

The overall conclusion was that the MPC approach was a preferred control methodology for the automatic needle insertion due to the described advantages over the PID control.

4 Discussion

4.1 Simulation

It was observed that the overall needle position error was lower than 1 mm. This level of precision ensures a clinically acceptable accuracy for the deposition of the radioactive seeds (less than ± 2 mm, as reported in [30]). Furthermore, the proposed control strategy resulted in minimizing the needle deflection, Fig. 6, so that the needle trajectories and, consequently, the radioactive sources were deposited in a straight line, allowing for several clinical advantages: a fast and more accurate needle reconstruction during the planning process in the interstitial brachytherapy practice, the decrease in the planning time reduces the time during which the patient is under anesthesia, the influence of anisotropy of the radioactive sources in prostate seed implants was minimized while it was possible to perform more accurate dose calculations, more accurate dose delivery to the tumorous tissue, etc. This level of accuracy is in the same range as in the previously reported accuracy range for robotic seed depositions in low-dose-rate brachytherapy [20, 24, 27, 29, 33, 35, 38, 45) or even improved. The accuracy obtained here is more favorable comparing to the reported values in the interstitial brachytherapy procedures (within 2.64 mm) [13]. This can be explained mostly by the prediction approach that includes the accurate mathematical modeling of the process and by the minimized disturbances in real time. In [20], the average transverse needle placement error was 2 mm, and the maximal error was 2.5 mm. The average sagittal error was 2.5 mm, and the maximal sagittal error 5.0 mm. The medial accuracy reported in [24] for the manual insertion technique was 1.8, 2.4 and 3.6 mm. A significant placement error reduction recorded in this study was previously noticed [7–9, 27] when the needle rotation was included. The insertion technique with needle rotation is not possible in the current standard clinical practice including the manual needle insertion performed by physicians. In addition, it was recorded that in the manual needle insertion the prostate (clinical target) could be displaced by up to 5.6 mm, and the robotic approach could significantly decrease this effect, to 0.9 mm [29]. In comparison with the manual methods, the decrease in the placement error in the automated procedures was reported to be 0.5, 0.2, 0.489, 1.44 and 1.2 mm in [6, 33, 35, 38, 45], respectively.

The rigorous simulation results (Figs. 6a, 7, 8) confirmed the decrease in the positioning error, possibility of the mathematical model, control system to correct for the change in the trajectory, decrease in the reactive forces and the torques for different ranges of the simulation parameters presented in Sect. 2.7. Therefore, the mathematical model, MPCN and its implementation demonstrated the consistency of the findings with the analyzed physical process. This novel method for the force control, prediction and minimization of the needle deflection is capable of driving the needle to the desired location. It shows strong potential for further investigations and clinical applications.

4.2 Influence of the needle placement errors on the clinical outcomes

The clinical justification of the described methodology for needle insertion is presented in the sequel. The purpose of this analysis was to investigate the influence of

Table 1 Influence of the needle placement errors on the dosimetry for PSI procedures

Target					Urethra		Rectum	
Constraints								
D90 [Gy] > 140	D90 > 90%	V100 ~90%	V150 < 70%	V200 < 30%	V125 < 1 cm^3	V150 0 cm^3	V69 < 8 cm^3	V100 < 1 cm^3
Original plan								
171.95	118.58	98.96	57.78	29.12	0.09	0	2.5	0.15
Plan with displacement								
170.30	117.45	99.18	56.56	28.52	0.01	0	2.85	0.34

the needle placement errors revealed in this study on the patients' dosimetry. Two representative clinical cases have been chosen for this purpose: the first was a prostate seed implant case in which the prescription dose was 145 Gy to the prostate, 24 needles and 76 radioactive I125 seeds with an apparent activity of 0.481 mCi were used; the second clinical case was an interstitial HDR brachytherapy implantation for uterine cancer, with a prescription dose of 2750 cGy in 5 fractions, delivered through 10 interstitial needles, tandem and two ovoids using an Utrecht applicator.

The analysis was performed by the comparison of the clinical plans with the corresponding plans in which the needles were randomly displaced for the maximum placement error (i.e., ± 1 mm) obtained in the simulation of needle insertion in this study. The changes in dosimetry were recorded and evaluated for both cases. Table 1 shows the results for the representative PSI case. The doses to the target (prostate) and to the organs at risk (rectum and urethra) were compared to the clinically acceptable values presented in the first row. It was concluded that the needle displacement error did not influence the final patient dosimetry. For the second case, it was noticed that the coverage of the clinical target volume was changed to 0.35%, and the dose to 2 cm^3 of the organs at risk (OER) (rectum, bladder and sigmoid) was changed to 0.24, 0.74 and 0.54%, respectively.

Consequently, the change in the dosimetric parameters was noticed to be at a level that, in general, does not influence the patient treatment outcomes. The differences in dosimetry did not translate to statistically significant dosimetric differences (both p values were greater than 0.5). To conclude, the noticed maximum needle positioning error obtained in this study did not influence the dosimetry of either the clinical targets or the OERs.

5 Conclusion

In this article, we presented a novel approach to the needle insertion. The controlled needle insertion using a predictive controller required a high-level mathematical model of the physical process. Due to that fact, the mathematical model of the robotic system with $(n + 2)$ DOF was presented. The needle was considered to be an elastic beam modeled with nDOF using the assumed-mode method. Using the adequate control methodology (MPC), it was possible to minimize the reactive force that was directly responsible for the needle deflection and needle tip displacement. Consequently, it was possible to guide the needle in a way which allowed for the maximum accuracy and minimal needle deflection.

The implementation of the proposed methodology can potentially improve the dosimetry in both the HDR and LDR brachytherapy procedures. This study reveals that the automatic needle insertion is feasible and efficacious. The automated needle insertion device delivers the needles into the desired location more precisely within a shorter period of time. With the use of an automated device for needle insertion with a properly chosen needle control methodology, the number of CT/MRI scans during HDR interstitial brachytherapy can be decreased. Consequently, the duration in which the patient is exposed to radiation during the diagnostic exams (CT) can decrease, and the patient may spend less time under anesthesia. The use of an automatic device for needle insertion during LDR prostate seed implants can result in more favorable dosimetry.

The future work will include the manufacturing of a mobile, portable and programmable robotic needle insertion mechanism with potential to be implemented in various medical procedures where the needle insertion must be performed with high reliability and accuracy, such as in interstitial brachytherapy, biopsy and other relevant procedures. The comparison between other control methodologies (different than presented PID approach) and the MPC can potentially lead to clinically relevant results. The non-rectilinear needle insertion including the variable reference can be additionally investigated. In addition, the clinical trials using the proposed device (animal and human) are part of the future work so that the limitations and the possible advantages of this device should be adequately addressed in various clinical settings.

References

1. Abolhassani N, Patel R, Moallem M (2004) Trajectory generation for robotic needle insertion in soft tissue. In: Proceedings of the 26th IEEE international conference on engineering in medicine and biology (EMBS), San Francisco CA, USA. pp 2730–2733
2. Abolhassani N, Patel R, Moallem M (2007) Needle insertion into soft tissue: a survey. Med Eng Phys 29(4):413–431
3. Alterovitz R, Goldberg K, Pouliot J, Taschereau R, Hsu IC (2003) Sensorless planning for medical needle insertion procedures. In: Proceedings of the IEEE/RSJ international conference on intelligent robots and systems, Las Vegas, NV, USA. pp 3337–3343
4. Alterovitz R, Goldberg K, Okamura A (2005) Planning for steerable bevel-tip needle insertion through 2D soft tissue with obstacles. In: Proceedings of IEEE international conference on robotics and automation (ICRA), Barcelona, Spain. pp 1640–1645
5. Asadian A, Patel RV, Kermani MR (2011) A distributed model for needle-tissue friction in percutaneous interventions. In: Proceedings of the IEEE international conference on robotics and automation (ICRA), Shanghai, China. pp 1896–1901
6. Buzurovic I et al (2008) Real-time control strategy for collision avoidance and seed deposition in brachytherapy robotic system. Int J Comput Assist Radiol Surg 3:30–34
7. Buzurovic I, Podder T, Yan K, Hu Y, Valicenti R, Dicker A, Yu Y (2008) Parameter optimization for brachytherapy robotic needle insertion and seed deposition. Med Phys 35(6):2865
8. Buzurovic I, Podder TK, Yu Y (2008) Force prediction and tracking for image-guided robotic system using neural network approach. In: Proceedings of IEEE biomedical circuits and systems conference (BioCAS), Baltimore MA, USA. pp 41–44
9. Buzurovic I, Podder TK, Yu Y (2010) Prediction control for brachytherapy robotic system. J Robot 2010(1):1–10
10. Buzurovic I, Debeljkovic D (2010) A geometric approach to the investigation of the dynamics of constrained robotic systems. In: Proceedings of IEEE international symposium on intelligent systems and informatics (SYSI), Subotica, Serbia. pp 133–138
11. Buzurovic I, Podder TK, Yu Y (2012) Robotic systems for radiation therapy. In: Dutta A (ed) Robotic systems—applications control and programming. InTech, Rijeka, pp 85–106
12. Baruh H (1998) Analytical dynamics. McGraw Hill, New York
13. Cepek J, Chronik BA, Lindner U, Trachtenberg J, Davidson SRH, Bax J, Fenster A (2013) A system for MRI-guided transperineal delivery of needles to the prostate for focal therapy. Med Phys 40(1):1–15
14. Chentanez N, Alterovitz R, Ritchie D, Cho L, Hauser KK, Goldberg K, O'Brien JF (2009) Interactive simulation of surgical needle insertion and steering. In: Proceedings of ACM SIGGRAPH, vol 28, no 3. pp 88:1–10
15. Chui CK, Teoh SH, Ong CJ, Anderson JH, Sakuma I (2006) Integrative modeling of liver organ for simulation of flexible needle insertion. In: Proceedings of the 9th international conference on control automation robotics *and* vision (ICARCV), Singapore. pp 1–6
16. Crouch JR, Schneider CM, Wainer J, Okamura AM (2005) Velocity-dependent model for needle insertion in soft tissue. In: Proceedings of the 2005 medical image computing and computer-assisted intervention (MICCAI 2005). pp 624–632
17. DiMaio SP, Salcudean SE (2002) Simulated interactive needle insertion. In: Proceedings of haptic interfaces for virtual environment and teleoperator systems (HAPTICS), Orlando FL, USA. pp 344–351
18. DiMaio SP, Salcudean SE (2003) Needle insertion modeling and simulation. IEEE Trans Robot Autom 19(5):864–875
19. DiMaio SP, Salcudean SE (2005) Interactive simulation of needle insertion models. IEEE Trans Biomed Eng 52(7):1167–1179
20. Fichtinger G, Burdette EC, Tanacs A, Patriciu A, Mazilu D, Whitcomb LL, Stoianovic D (2006) Robotically assisted prostate brachytherapy with transrectal ultrasound guidance—phantom experiments. Brachytherapy 5:14–26
21. Holden MS, Ungi T, Sargent D, McGraw RC, Fichtinger G (2012) Surgical motion characterization in simulated needle insertion procedures. In: Proceedings of SPIE medical imaging: image-guided procedures, robotic interventions, and modeling, vol 8316
22. Khadem M, Fallahi B, Rossa C, Sloboda RS, Usmani N, Tavakoli M (2015) A mechanics-based model for simulation and control of flexible needle insertion in soft tissue. In: Proceedings of the IEEE international conference on robotics and automation (ICRA), Seattle, USA. pp 2264–2269
23. Kobayashi Y, Suzuki M, Kato A, Hatano M, Konishi K, Hashizume M, Fujie MG (2012) Enhanced targeting in breast tissue using a robotic tissue preloading-based needle insertion system. IEEE Trans Robot Autom 28(3):710–722
24. Lin A, Trejos AL, Patel RV, Malthaner RA (2008) Robot-assisted minimally invasive brachytherapy for lung cancer. Telesurgery. pp 35–52
25. McGill CS, Schwartz JA, Moore JZ, McLaughlin PW, Shih AJ (2012) Effects of insertion speed and trocar stiffness on the accuracy of needle position for brachytherapy. Med Phys 39:1811–1817
26. Meirovitch L (2001) Fundamentals of vibrations. McGraw Hill, New York
27. Meltsner MA, Ferrier NJ, Thomadsen BR (2007) Observations on rotating needle insertions using a brachytherapy robot. Phys Med Biol 52:6027–6037
28. Misra S, Reed KB, Schafer BW, Ramesh KT, Okamura AM (2010) Mechanics of flexible needles robotically steered through soft tissue. Int J Robot Res 29(13):1640–1660
29. Moerland MA, Van den Bosch MR, Lagerburg V, Battermann JJ, Van Vulpen M, Lagendijk JJW (2008) An MRI scanner compatible implant robot for prostate brachytherapy. Brachytherapy 7(2):100
30. Nath R, Anderson LL, Meli JA, Olch AJ, Stitt JA, Williamson JF (1997) Code of practice for brachytherapy physics: report of the AAPM radiation therapy committee task group No. 56. Med Phys 24(10):1557–1598
31. O'Leary MD, Simone C, Washio T, Yoshinaka K, Okamura AM (2003) Robotic needle insertion: effects of friction and needle geometry. In: Proceedings of IEEE international conference on robotics and automation (ICRA), Taipei, Taiwan. pp 1774–1780
32. Okamura AM, Simone C, O'Leary MD (2004) Force modeling for needle insertion into soft tissue. IEEE Trans Biomed Eng 51(10):1707–1716
33. Podder T, Buzurovic I, Yu Y (2010) Multichannel robot for image-guided brachytherapy. In: Proceedings of the 10th IEEE international conference on bioinformatics and bioengineering (BIBE), Philadelphia PA, USA. pp 209–213
34. Roesthuis RJ, van de Berg NJ, van den Dobbelsteen JJ, Misra S (2015) Modeling and steering of a novel actuated-tip needle through a soft-tissue simulant using Fiber Bragg Grating sensors. In: Proceedings of the IEEE international conference on robotics and automation (ICRA), Seattle, USA. pp 2283–2289
35. Salcudean SE, Prananta TD, Morris WJ, Spadinger I (2008) Robotic needle guide for prostate brachytherapy. In: IEEE international conference on robotics and automation (ICRA), Pasadena CA, USA. pp 2975–2981
36. Siebert FA, Hirt M, Niehoff P, Kovács G (2004) Imaging of implant needles for real-time HDR-brachytherapy prostate treatment using biplane ultrasound transducers. Med Phys 36(8):3406–3412

37. Simone C, Okamura AM (2002) Modeling of needle insertion forces for robot-assisted percutaneous therapy. In: Proceedings of IEEE international conference on robotics and automation (ICRA), Washington DC, USA. pp 2085–2091
38. Stoianovici D, Cleary K, Patriciu A, Mazilu D, Stanimir A, Craciunoiu N, Watson V, Kavoussi L (2003) AcuBot: a robot for radiological percutaneous interventions. IEEE Trans Robot Autom 19:927–930
39. Swensen JP, Cowan NJ (2012) Torsional dynamics compensation enhances robotic control of tip-steerable needles. In: Proceedings of the IEEE international conference on robotics and automation (ICRA), Saint Paul, USA. pp 1601–1606
40. Theodore RJ, Ghosal A (1995) Comparison of the assumed modes and finite element models for flexible multilink manipulators. Int J Robot Res 14(2):91–111
41. Vrooijink GJ, Abayazid M, Misra S (2013) Real-time three-dimensional flexible needle tracking using two-dimensional ultrasound. In: Proceedings of the IEEE international conference on robotics and automation (ICRA), Karlsruhe, Germany. pp 1688–1693
42. Wedlick TR, Okamura AM (2012) Characterization of robotic needle insertion and rotation in artificial and ex vivo tissues. In: Proceedings of IEEE/RAS-EMBS international conference on biomedical robotics and biomechatronics (BioRob), Roma, Italy. pp 62–68
43. Wedlick TR, Lin DJ, Okamura AM (2013) Tissue fixation by suction increases the accuracy of robotic needle insertion. In: Proceedings of IEEE international conference on robotics and automation (ICRA), Karlsruhe, Germany. pp 1694–1699
44. Wan G, Wei Z, Gardi L, Downey D, Fenster A (2005) Brachytherapy needle deflection evaluation and correction. Med Phys 32(4):902–909
45. Wei Z, Wan G, Gardi L, Mills G, Downey D, Fenster A (2004) Robot-assisted 3D-TRUS guided prostate brachytherapy: system integration and validation. Med Phys 31:539–548

Ivan M. Buzurovic is Instructor of Medical Physics, Harvard Medical School, Boston MA, USA. His research fields are medical physics, control systems, medical robotics and mathematical modeling and simulations.

Slavisa Salinic is Associate Professor of Mechanical Engineering. He is with Department of Mechanics, Faculty of Mechanical and Civil Engineering in Kraljevo, University of Kragujevac, Serbia.

Peter F. Orio is Assistant Professor of Radiation Oncology, Harvard Medical School. He is Chair of Network Operations, Department of Radiation Oncology, Boston MA, USA, and Director-at-Large of American Brachytherapy Society.

Paul L. Nguyen is Associate Professor of Radiation Oncology, Harvard Medical School. He is director of Prostate Brachytherapy and Clinical Trials for Genitourinary Radiation Oncology, Dana-Farber Cancer Institute, Boston MA, USA.

Robert A. Cormack is Assistant Professor of Medical Physics, Harvard Medical School and Vice Chair of Medical Physics and Biophysics Division of Dana-Farber/Brigham and Women's Cancer Center, Boston MA, USA.